Inorganic Chemistry

Article

pubs.acs.org/IC

Metastable Interwoven Mesoporous Metal–Organic Frameworks

Yabing He,*[,†,‡] Zhiyong Guo,[‡] Shengchang Xiang,[§] Zhangjing Zhang,[§] Wei Zhou,[≠,±] Frank R. Fronczek,[∥] Sean Parkin,[¶] Stephen T. Hyde,[◊] Michael O'Keeffe,[△] and Banglin Chen*[,‡]

[†]College of Chemistry and Life Sciences, Zhejiang Normal University, Jinhua 321004, China

[‡]Department of Chemistry, University of Texas at San Antonio, One UTSA Circle, San Antonio, Texas 78249-0698, United States

[§]College of Chemistry and Material, Fujian Normal University, 3 Shangsan Road, Cangshang Region, Fuzhou 350007, China

[≠]NIST Center for Neutron Research, Gaithersburg, Maryland 20899-6102, United States

[±]Department of Materials Science and Engineering, University of Maryland, College Park, Maryland 20742, United States

[∥]Department of Chemistry, Louisiana State University, Baton Rouge, Louisiana 70803-1804, United States

[¶]Department of Chemistry, University of Kentucky, Lexington, Kentucky 40506-0055, United States

[◊]Department of Applied Mathematics, Australian National University, Canberra, Australia

[△]Department of Chemistry and Biochemistry, Arizona State University, Tempe, Arizona 85287-1604, United States

Supporting Information

ABSTRACT: Three isostructural interwoven 3,4-connected mesoporous metal–organic frameworks of pto-a topology (**UTSA-28-Cu**, **UTSA-28-Zn**, and **UTSA-28-Mn**) were synthesized and structurally characterized. Because of their metastable nature, their gas sorption properties are highly dependent on the metal ions and activation profiles. The most stable, **UTSA-28a-Cu**, exhibits promising gas storage and separation capacities.

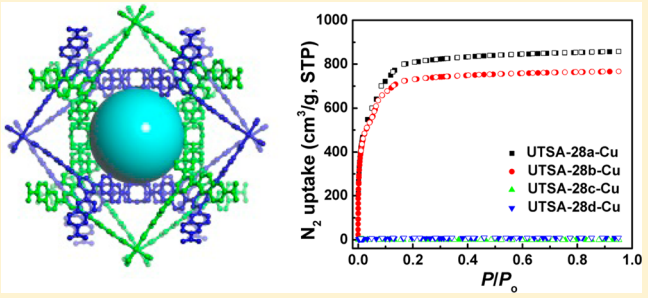

INTRODUCTION

Metal–organic frameworks (MOFs) and/or porous coordination polymers (PCPs) are a new class of porous materials that have been widely studied not only for their fascinating structures but, more importantly, for their diverse applications in gas storage and separation, catalysis, sensing, and drug delivery.[1,2] The establishment of their permanent porosities is necessary for us to explore the above-mentioned properties; thus, extensive research has been pursued to stabilize the frameworks. Unlike the ionic bonds in the sophisticated zeolite porous materials, the coordination bonds to generate the MOFs are much weaker, leading to their unique structure features such as framework flexibility and metastability. Because of these, the establishment of their permanent porosities is not only dependent on their structures but also dependent on the activation profiles, particularly for those mesoporous MOFs.[3] In fact, a few mesoporous MOFs whose gas sorption cannot be established through conventional activation have been confirmed to take up a large amount of gas molecules through activation with supercritical carbon dioxide.[4] We report herein three isostructural interwoven mesoporous MOFs (**UTSA-28-Cu**, **UTSA-28-Zn**, and **UTSA-28-Mn**) that are assembled from the new BTN linker (H_3BTN = 6,6′,6″-benzene-1,3,5-triyl-2,2′,2″-trinaphthoic acid; Scheme 1) and binuclear $M_2(CO_2)_4$ (M = Cu^{2+}, Zn^{2+}, and Mn^{2+}) paddlewheel secondary building units (SBUs). This new expanded BTB (H_3BTB = 4,4′,4″-benzene-1,3,5-triyltribenzoic acid) organic linker has enlarged the cages of 16.4 Å in **MOF-14** [$Cu_3(BTB)_2(H_2O)_3$] to those of 25.6 Å in **UTSA-28**. More interestingly, this series of mesoporous MOFs exhibits framework metastability attributed to their interwoven structures, so their permanent porosities are not only dependent on the metal ions but also dependent on the activation profiles. The establishment of a high porosity (Brunauer–Emmett–Teller, BET = 3179 m^2 g^{-1}) of **UTSA-28a-Cu** has enabled it to take up a large amount of CH_4 [total of 197.3 cm^3 (STP) g^{-1} at 300 K and 46 bar] and CO_2 [total of 413 cm^3 (STP) g^{-1} at 300 K and 28 bar].

EXPERIMENTAL SECTION

Materials and Measurements. All reagents and solvents were used as received from commercial suppliers without further purification. Fourier transform infrared (FTIR) spectra were performed on a Bruker Vector 22 spectrometer at room temperature. The elemental analyses were performed with Perkin-Elmer 240 CHN analyzers from Galbraith Laboratories, Knoxville, TN. Thermogravimetric analyses (TGA) were measured using a Shimadzu TGA-50 analyzer under a nitrogen atmosphere with a heating rate of 3 °C min^{-1}. Powder X-ray diffraction (PXRD) patterns were recorded by a

Received: July 25, 2013
Published: September 25, 2013

dx.doi.org/10.1021/ic401870e | Inorg. Chem. 2013, 52, 11580–11584

Scheme 1. Synthesis of MOFs

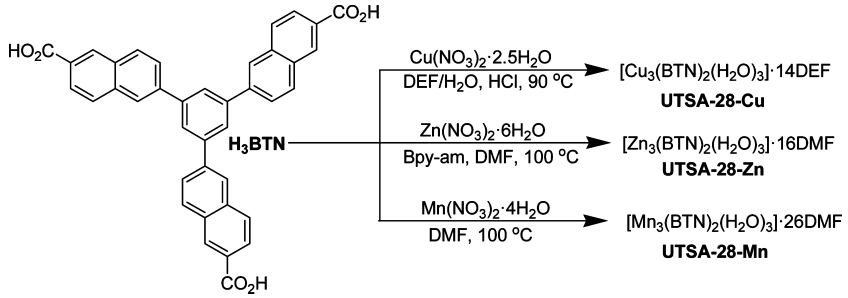

Rigaku Ultima IV diffractometer operated at 40 kV and 44 mA with a scan rate of 1.0 deg min^{-1}. A Micromeritics ASAP 2020 surface area analyzer was used to measure gas adsorption isotherms. The samples were maintained at 77 K with liquid nitrogen and at 273 K with an ice–water bath. Because the center-controlled air condition was set up at 23 °C, a water bath was used for adsorption isotherms at 296 K. High-pressure sorption isotherms were measured using a Sieverts-type apparatus.

Single-Crystal X-ray Structure Determination. Crystal data were collected on a Bruker SMART Apex II CCD-based X-ray diffractometer system equipped with a Mo or Cu target X-ray tube. *PLATON/SQUEEZE* was employed to calculate the diffraction contribution of the solvent molecules and thereby produce a set of solvent-free diffraction intensities. The structure was solved by direct methods and refined to convergence by a least-squares method on F^2 using the *SHELXTL* software suite. The H atoms on the ligands were placed in idealized positions and refined using a riding model. CCDC 951329–951331 contain the supplementary crystallographic data for **UTSA-28-Cu**, **UTSA-28-Zn**, and **UTSA-28-Mn**. The data can be obtained free of charge from The Cambridge Crystallographic Data Centre via www.ccdc.cam.ac.uk/data_request/cif.

Synthesis and Characterization of UTSA-28-Cu. A mixture of H_3BTN (8.3 mg, 14.2 μmol) and $Cu(NO_3)_2·2.5H_2O$ (14.5 mg, 62.3 μmol, Aldrich) was dissolved in a mixed solvent of *N*,*N*′-diethylformamide (DEF; 1.0 mL) and H_2O (0.1 mL) in a disposable scintillation vial (20 mL). Upon the addition of 10 μL of 6 M HCl, the vial was capped and heated at 90 °C for 24 h. The polyhedral crystals were collected in 71% yield. **UTSA-28-Cu** was best formulated as $[Cu_3(BTN)_2(H_2O)_3]·14DEF$. Selected FTIR (neat, cm^{-1}): 1653, 1616, 1614, 1482, 1439, 1400, 1398, 1379, 1363, 1309, 1263, 1261, 1216, 1214, 1109, 1107, 944, 922, 879, 822, 781, 764, 754, 705. TGA data. Calcd weight loss for 14DEF and $3H_2O$: 51.9. Found: 52.4. Anal. Calcd for $C_{148}H_{202}N_{14}O_{29}Cu_3$: C, 62.77; H, 7.19; N, 6.92. Found: C, 63.01; H, 7.23; N, 6.77.

Synthesis and Characterization of UTSA-28-Zn. A mixture of H_3BTN (14.7 mg, 25.1 μmol), *N*-(pyridin-4-yl)isonicotinamide (Bpy-am; 5.4 mg, 27.1 μmol), and $Zn(NO_3)_2·6H_2O$ (29.7 mg, 99.8 μmol, Aldrich) was dissolved into 1.5 mL of *N*,*N*′-dimethylformamide (DMF) in a disposable scintillation vial (20 mL). The vial was capped and heated at 100 °C for 24 h. The block-shaped crystals were collected by in 55% yield. **UTSA-28-Zn** was best formulated as $[Zn_3(BTN)_2(H_2O)_3]·16DMF$. Selected FTIR (neat, cm^{-1}): 1652, 1599, 1497, 1480, 1437, 1384, 1332, 1300, 1253, 1213, 1136, 1091, 1062, 1031, 975, 920, 902, 878, 864, 824, 780, 763, 751, 702, 658. TGA data. Calcd weight loss for 16DMF and $3H_2O$: 47.2. Found: 46.9. Anal. Calcd for $C_{126}H_{160}N_{16}O_{31}Zn_3$: C, 58.41; H, 6.22; N, 8.65. Found: C, 58.23; H, 6.03; N, 8.74.

Synthesis and Characterization of UTSA-28-Mn. A mixture of H_3BTN (10.0 mg, 17.1 μmol) and $Mn(NO_3)_2·4H_2O$ (25.0 mg, 99.6 μmol, Alfa) was dissolved into 1.5 mL of DMF in a disposable scintillation vial (20 mL). The vial was capped and heated at 100 °C for 1 week. The cubic-shaped crystals were collected in 23% yield. **UTSA-28-Mn** was best formulated as $[Mn_3(BTN)_2(H_2O)_3]·26DMF$. Selected FTIR (neat, cm^{-1}): 1646, 1607, 1582, 1544, 1479, 1436, 1374, 1252, 1214, 1136, 1094, 1061, 964, 918, 875, 813, 778, 748, 703, 659. TGA data. Calcd weight loss for 26DMF and $3H_2O$: 59.4. Found: 59.1. Anal. Calcd for $C_{156}H_{230}N_{26}O_{41}Mn_3$: C, 56.94; H, 7.05; N, 11.07. Found: C, 56.50; H, 7.21; N, 10.75.

RESULTS AND DISCUSSION

The C_3-symmetric organic linker H_3BTN was readily synthesized by palladium-catalyzed Suzuki cross-coupling between 1,3,5-tribromobenzene and methyl 6-(pinacolboryl)-2-naphthoate followed by hydrolysis and acidification in good yield. Solvothermal reaction between H_3BTN and $Cu(NO_3)_2·2.5H_2O$ in a DEF/H_2O mixture under acidic conditions at 90 °C for 24 h afforded blue polyhedral-shaped single crystals of **UTSA-28-Cu** ($[Cu_3(BTN)_2(H_2O)_3]·14DEF$). **UTSA-28-Zn** ($[Zn_3(BTN)_2(H_2O)_3]·16DMF$) was obtained as colorless block-shaped crystals via a solvothermal reaction between H_3BTN and $Zn(NO_3)_2·6H_2O$ in DMF in the presence of Bpy-am, while **UTSA-28-Mn** ($[Mn_3(BTN)_2(H_2O)_3]·26DMF$) was synthesized by a solvothermal reaction of H_3BTN and $Mn(NO_3)_2·4H_2O$ in DMF for 1 week. Their structures were determined by single-crystal X-ray diffraction analysis, and the phase purity of the bulk materials was confirmed by PXRD (Figures S1–S3 in the Supporting Information, SI). The formulas were established based on single-crystal X-ray diffraction studies, TGA (Figure S4 in the SI), and micro-analysis.

Because the single-crystal X-ray studies and PXRD experiments confirmed that they are isostructural, the crystal structure of **UTSA-28-Cu** was representatively described. **UTSA-28-Cu** is an interwoven 3D framework that crystallizes in a cubic space group $Pn\bar{3}n$. Each framework is composed of in situ formed square-planar dicopper paddlewheel SBUs that are linked by triangular BTN units to form a 3,4-connected net with pto topology (Figure 1a,b),[5] where the BTN unit serves as a 3-connected node and the dicopper paddlewheel SBU serves as planar 4-connected node. The naphthalene ring in the organic linker is twisted from the center benzene ring with a dihedral angle of 36.5°. A pair of frameworks are interwoven in each other. There exist weak π–π interactions between the two center benzene rings from two interpenetrating networks with a center-to-center distance of about 3.9 Å (Figure 1c–f). Because BTN is larger than BTB, the cages of 25.6 Å in **UTSA-28-Cu** are larger than those of 16.4 Å in **MOF-14**.[6] Accordingly, **UTSA-28-Cu** also has larger effective window sizes of about 11.1 × 11.1 $Å^2$. The total accessible volume in **UTSA-28-Cu** was calculated using *PLATON* to be 73.86% after removal of guest solvents and coordinated H_2O molecules.[7]

Different activation methods were used to determine the permanent porosity by N_2 adsorption at 77 K. The as-synthesized **UTSA-28-Cu** was guest-exchanged with dry acetone, dichloromethane, and methanol, respectively, followed by activation at room temperature under high vacuum

dx.doi.org/10.1021/ic401870e | *Inorg. Chem.* 2013, 52, 11580–11584

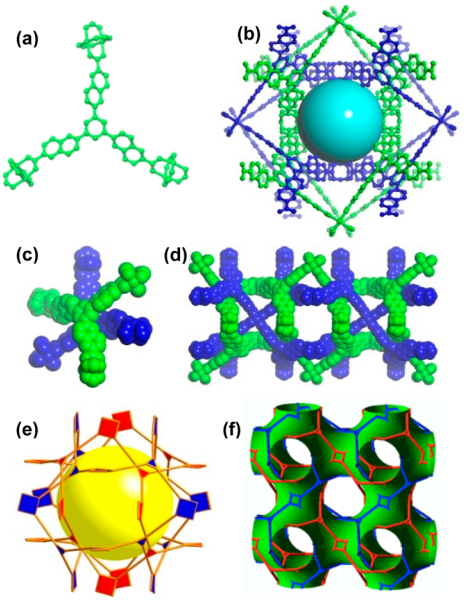

Figure 1. Single-crystal X-ray structure of **UTSA-28-Cu** indicating that square paddlewheel SBUs were linked by triangular BTN units (a) to form a pair of interwoven 3D porous frameworks (b and f) with pto-a topology (e) that are held together by numerous $\pi-\pi$ and CH$-\pi$ interactions (c and d).

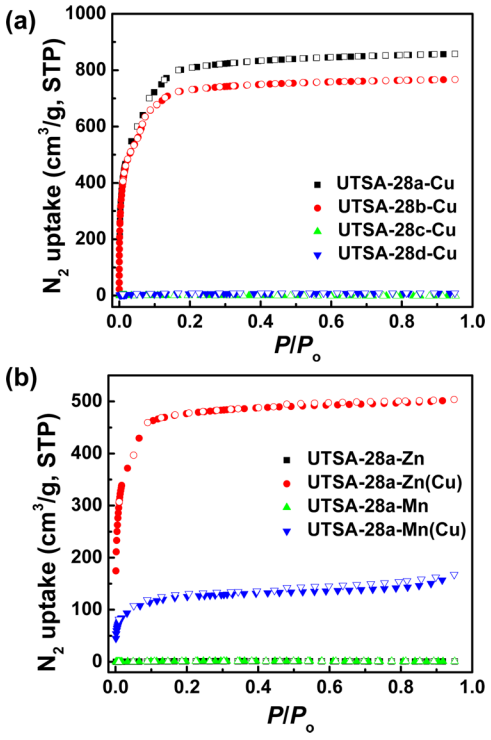

Figure 2. N_2 sorption isotherms at 77 K for (a) the activated **UTSA-28a-Cu**, **UTSA-28b-Cu**, **UTSA-28c-Cu**, and **UTSA-28d-Cu** and for (b) the activated **UTSA-28a-Zn**, **UTSA-28a-Mn**, **UTSA-28a-Zn(Cu)**, and **UTSA-28a-Mn(Cu)**. The solid and open symbols represent the adsorption and desorption data, respectively.

overnight to get the activated **UTSA-28a-Cu**, **UTSA-28b-Cu**, and **UTSA-28c-Cu**, respectively. **UTSA-28d-Cu** was prepared through freeze-drying activation in which the freshly benzene-exchanged **UTSA-28-Cu** was activated at 0 °C overnight, followed by activation for 24 h at room temperature.[8]

The N_2 sorption isotherms of all activated samples are shown in Figure 2a, and the corresponding BET and Langmuir surface areas as well as pore volumes are listed in Table S1 in the SI. The significantly different N_2 sorption isotherms of these samples are attributed to the metastable nature of **UTSA-28-Cu**. The most surprising are the facts that **UTSA-28c-Cu** and **UTSA-28d-Cu**, generated from the freshly methanol- and benzene-exchanged samples, respectively, do not take up any N_2 molecule at all. The exact reason is not very clear; we speculate that the strong interactions between the guest methanol molecules with the framework (particularly the terminal H_2O molecules) among **UTSA-28c-Cu** and the strong aromatic $\pi-\pi$ interactions between the guest benzene molecules with the BTN organic linkers within the framework **UTSA-28d-Cu** play a crucial role. Using acetone as the activation solvent produced the most porous framework: the activated **UTSA-28a-Cu** exhibits BET and Langmuir surface areas of 3179 and 3957 $m^2\ g^{-1}$, respectively. These values are about twice those in **MOF-14**. The pore volume calculated from the maximum amount of N_2 adsorbed is 1.33 $cm^3\ g^{-1}$.

It is understandable that **UTSA-28a-Zn** and **UTSA-28a-Mn** do not take up any N_2 molecule because the $Zn_2(CO_2)_4$ and $Mn_2(CO_2)_4$ SBUs are not as rigid as the $Cu_2(CO_2)_4$ one to stabilize the frameworks. In fact, even the **HKUST-1** analogue $Zn_3(BTC)_2$ is not porous at all.[9] Inspired by the recent reports that the $Zn_2(CO_2)_4$ SBUs in a MOF can be substituted by the $Cu_2(CO_2)_4$ ones via postsynthetic metal-ion exchange,[10] we prepared the Cu^{II}-substituted **UTSA-28-Zn** and **UTSA-28-Mn**, namely, **UTSA-28-Zn(Cu)** and **UTSA-28-Mn(Cu)**, respectively. When the as-synthesized **UTSA-28-Zn** were immersed in a 0.1 M methanol solution of $Cu(NO_3)_2{\cdot}2.5H_2O$ at room temperature for 1 week, the original colorless crystals turned to green-blue ones while maintaining their original shapes and sizes (Figure S6 in the SI), indicating a clean single-crystal-to-single-crystal transformation. Inductively coupled plasma analysis of the metal-ion-exchanged sample **UTSA-28-Zn(Cu)** indicates that up to 80% of Zn ions in the framework were exchanged by Cu^{II} ions over 1 week. The PXRD studies confirmed that the framework was preserved during the metal-ion exchange process (Figure S7 in the SI). In addition, no stretching band corresponding to the nitrate anion was detected in FTIR spectra of **UTSA-28-Zn(Cu)**, demonstrating that there was no Cu^{II} ion absorbed in the pore channels (Figure S8 in the SI). The acetone-exchanged **UTSA-28-Zn(Cu)** was activated under vacuum at room temperature to investigate its porosity. Remarkably, **UTSA-28a-Zn(Cu)** shows significantly improved gas sorption properties compared to the original **UTSA-28a-Zn** (Figure 2b and Table S1 in the SI). N_2 uptake of **UTSA-28a-Zn(Cu)** reaches 504 $cm^3\ g^{-1}$ at 1 atm at 77 K, corresponding to a BET surface area of 1890 $m^2\ g^{-1}$. The permanent porosity of the activated **UTSA-28a-Mn(Cu)** has also been established (Figure 2b and Table S1 in the SI).

Establishment of the permanent porosity of **UTSA-28a-Cu** encourages us to explore its gas storage and separation capacities. Because of its high porosities, the high-pressure CO_2, CH_4, and H_2 adsorptions up to 60 bar were measured at the Center for Neutron Research, National Institute of Standards and Technology (NIST), using a computer-controlled Sieverts apparatus (Figure 3a). The H_2 adsorption isotherm of **UTSA-28a-Cu** shows a maximum excess uptake of 3.9 wt % at 33 bar and 77 K (Figure S9a in the SI). Using the N_2-derived pore volume and the bulk phase density of H_2, the total H_2 uptake at 77 K and 52 bar was calculated to be 5.0 wt

dx.doi.org/10.1021/ic401870e | *Inorg. Chem.* 2013, 52, 11580−11584

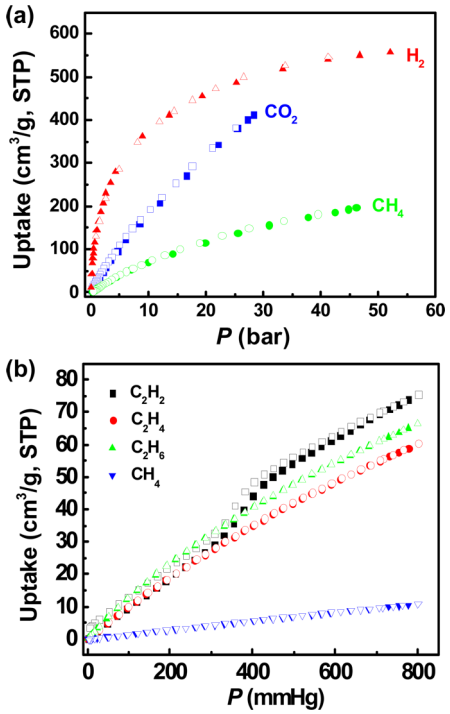

Figure 3. (a) Absolute high-pressure CO_2 (300 K), CH_4 (300 K), and H_2 (77 K) sorption isotherms of **UTSA-28a-Cu**. (b) C_2H_2, C_2H_4, C_2H_6, and CH_4 sorption isotherms of **UTSA-28a-Cu** at 296 K. The solid and open symbols represent the adsorption and desorption data, respectively.

% (Figure S9b in the SI), which is moderate compared with the highest-capacity MOF materials.[4] At 35 bar and 300 K, the excess and absolute CH_4 uptakes of **UTSA-28a-Cu** reach 149.2 and 167.9 cm^3 (STP) g^{-1}, respectively. The total methane uptake can increase to 197.3 cm^3 (STP) g^{-1} at 300 K and 46 bar (Figures 3a and S10 in the SI). The total CO_2 adsorption capacity is 81.1 wt % [413 cm^3 (STP) g^{-1}] at 300 K and 28 bar (Figures 3a and S11 in the SI), which is moderately high.

We have recently paid much attention to porous MOFs for the storage and separation of small hydrocarbons because of their very important industrial applications.[11] Accordingly, the pure-component small hydrocarbon sorption isotherms for **UTSA-28a-Cu** were measured. As shown in Figures 3b and S12 in the SI, all isotherms show reversible sorption behavior. Remarkably, **UTSA-28a-Cu** systematically takes up much more C_2 hydrocarbons than C_1 methane. At 296 K, **UTSA-28a-Cu** takes up a moderate amount of C_2H_2 (87.6 mg g^{-1}), C_2H_4 (75.5 mg g^{-1}), and C_2H_6 (89.1 mg g^{-1}), but basically a negligible amount of CH_4 (7.7 mg g^{-1}) at 1 atm, indicating **UTSA-28a-Cu** as a promising material for the adsorptive separation of C_2 hydrocarbons from methane at room temperature. The preferable adsorption of C_2 hydrocarbons relative to C_1 methane is attributed to the stronger interaction of the framework with C_2 hydrocarbons because no molecule sieving effect exists in **UTSA-28a-Cu** because the size of the open channel is much bigger than that of gas molecules. The Henry's law selectivities for C_2H_2, C_2H_4, and C_2H_6 over CH_4 at 296 K are 9.2, 8.6, and 13.2, respectively, which are moderate compared with those of the best-performing materials **FeMOF-74**, **CoMOF-74**, and **MgMOF-74**.[11a,12] Nevertheless, the low isosteric heat of adsorption at zero coverage (16.9−25.6 kJ mol^{-1}; Table S2 in the SI), calculated by fitting experimental isotherm data at 273 and 296 K to the virial equation, indicates the low regeneration cost. The large pore volume of **UTSA-28a-Cu** will also secure its large separation capacities for the small hydrocarbons. In practical applications, both separation selectivity and capacity should be balanced to optimize the separation efficiency.

CONCLUSION

In summary, we synthesized three isostructural interwoven MOFs based on a new C_3-symmetrical aromatic tricarboxylate of pto-a topology. The large pore space of 25.6 Å in the mesoporous regime and weak interactions between the two interwoven frameworks lead to their metastable structure features, so their framework stability and gas sorption properties were heavily dependent on the metal ions and activation profiles. The most stable **UTSA-28a-Cu** exhibits the potential for gas storage and separation. Our work thus demonstrates the significance of the activation profiles on control of the framework stability and porosity.

ASSOCIATED CONTENT

Supporting Information

PXRD, TGA, gas sorption isotherms, FTIR, sorption data under different activation methods, virial analysis data, crystal data and structure refinement, and CIF files. This material is available free of charge via the Internet at http://pubs.acs.org.

AUTHOR INFORMATION

Corresponding Authors

*E-mail: heyabing@gmail.com.
*E-mail: banglin.chen@utsa.edu.

Author Contributions

The manuscript was written through contributions of all authors. All authors have given approval to the final version of the manuscript.

Notes

The authors declare no competing financial interest.

ACKNOWLEDGMENTS

This work was supported by Award AX-1730 from the Welch Foundation (to B.C.).

REFERENCES

(1) (a) He, Y.; Zhou, W.; Krishna, R.; Chen, B. *Chem. Commun.* **2012**, *48*, 11813−11831. (b) Suh, M. P.; Park, H. J.; Prasad, T. K.; Lim, D.-W. *Chem. Rev.* **2012**, *112*, 782−835. (c) Lin, X.; Champness, N. R.; Schröder, M. *Top. Curr. Chem.* **2010**, *293*, 35−76. (d) Ma, S.; Zhou, H.-C. *Chem. Commun.* **2010**, *46*, 44−53. (e) Makal, T. A.; Li, J.-R.; Lu, W.; Zhou, H.-C. *Chem. Soc. Rev.* **2012**, *41*, 7761−7779. (f) Getman, R. B.; Bae, Y.-S.; Wilmer, C. E.; Snurr, R. Q. *Chem. Rev.* **2012**, *112*, 703−723. (g) Li, J.-R.; Sculley, J.; Zhou, H.-C. *Chem. Rev.* **2012**, *112*, 869−932. (h) Sumida, K.; Rogow, D. L.; Mason, J. A.; McDonald, T. M.; Bloch, E. D.; Herm, Z. R.; Bae, T.-H.; Long, J. R. *Chem. Rev.* **2012**, *112*, 724−781. (i) Wu, H.; Gong, Q.; Olson, D. H.; Li, J. *Chem. Rev.* **2012**, *112*, 836−868. (j) Yoon, M.; Srirambalaji, R.; Kim, K. *Chem. Rev.* **2012**, *112*, 1196−1231. (k) Chen, B.; Xiang, S.; Qian, G. *Acc. Chem. Res.* **2010**, *43*, 1115−1124. (l) Cui, Y.; Yue, Y.; Qian, G.; Chen, B. *Chem. Rev.* **2012**, *112*, 1126−1162. (m) Kreno, L. E.; Leong, K.; Farha, O. K.; Allendorf, M.; Duyne, R. P. V.; Hupp, J. T. *Chem. Rev.* **2012**, *112*, 1105−1125. (n) Allendorf, M. D.; Bauer, C. A.; Bhakta, R. K.; Houk, R. J. T. *Chem. Soc. Rev.* **2009**, *38*, 1330−1352. (o) Horcajada, P.; Gref, R.; Baati, T.; Allan, P. K.; Maurin, G.; Couvreur, P.; Férey, G.; Morris, R. E.; Serre, C. *Chem. Rev.* **2012**, *112*, 1232−1268. (p) Kitagawa, S.; Kitaura, R.; Noro, S.-i. *Angew. Chem., Int.*

Ed. **2004**, *43*, 2334−2375. (q) Yaghi, O. M.; O'Keeffe, M.; Ockwig, N. W.; Chae, H. K.; Eddaoudi, M.; Kim, J. *Nature* **2003**, *423*, 705−714.
(2) (a) Nugent, P.; Belmabkhout, Y.; Burd, S. D.; Cairns, A. J.; Luebke, R.; Forrest, K.; Pham, T.; Ma, S.; Space, B.; Wojtas, L.; Eddaoudi, M.; Zaworotko, M. J. *Nature* **2013**, *495*, 80−84. (b) Vaidhyanathan, R.; Iremonger, S. S.; Shimizu, G. K. H.; Boyd, P. G.; Alavi, S.; Woo, T. K. *Science* **2010**, *330*, 650−653. (c) Xue, D.-X.; Cairns, A. J.; Belmabkhout, Y.; Wojtas, L.; Liu, Y.; Alkordi, M. H.; Eddaoudi, M. *J. Am. Chem. Soc.* **2013**, *135*, 7660−7667. (d) Caskey, S. R.; Wong-Foy, A. G.; Matzger, A. J. *J. Am. Chem. Soc.* **2008**, *130*, 10870−10871. (e) Gedrich, K.; Senkovska, I.; Klein, N.; Stoeck, U.; Henschel, A.; Lohe, M. R.; Baburin, I. A.; Mueller, U.; Kaskel, S. *Angew. Chem., Int. Ed.* **2010**, *49*, 8489−8492. (f) Panda, T.; Pachfule, P.; Chen, Y.; Jiang, J.; Banerjee, R. *Chem. Commun.* **2011**, *47*, 2011−2013. (g) Lin, Q.; Wu, T.; Zheng, S.-T.; Bu, X.; Feng, P. *J. Am. Chem. Soc.* **2012**, *134*, 784−787. (h) Zhang, J.-P.; Chen, X.-M. *J. Am. Chem. Soc.* **2009**, *131*, 5516−5521. (i) Jiang, H.-L.; Xu, Q. *Chem. Commun.* **2011**, *47*, 3351−3370. (j) Wu, H.; Zhou, W.; Yildirim, T. *J. Am. Chem. Soc.* **2009**, *131*, 4995−5000. (k) He, Y.; Zhou, W.; Yildirim, T.; Chen, B. *Energy Environ. Sci.* **2013**, *6*, 2735−2744.
(3) (a) Fang, Q.-R.; Makal, T. A.; Young, M. D.; Zhou, H.-C. *Comments Inorg. Chem.* **2010**, *31*, 165−195. (b) Xuan, W.; Zhu, C.; Liu, Y.; Cui, Y. *Chem. Soc. Rev.* **2012**, *41*, 1677−1695. (c) Song, L.; Zhang, J.; Sun, L.; Xu, F.; Li, F.; Zhang, H.; Si, X.; Jiao, C.; Li, Z.; Liu, S.; Liu, Y.; Zhou, H.; Sun, D.; Du, Y.; Cao, Z.; Gabelica, Z. *Energy Environ. Sci.* **2012**, *5*, 7508−7520. (d) Park, Y. K.; Choi, S. B.; Kim, H.; Kim, K.; Won, B.-H.; Choi, K.; Choi, J.-S.; Ahn, W.-S.; Won, N.; Kim, S.; Jung, D. H.; Choi, S.-H.; Kim, G.-H.; Cha, S.-S.; Jhon, Y. H.; Yang, J. K.; Kim, J. *Angew. Chem., Int. Ed.* **2007**, *46*, 8230−8233.
(4) (a) Farha, O. K.; Yazaydın, A. Ö.; Eryazici, I.; Malliakas, C. D.; Hauser, B. G.; Kanatzidis, M. G.; Nguyen, S. T.; Snurr, R. Q.; Hupp, J. T. *Nat. Chem.* **2010**, *2*, 944−948. (b) Furukawa, H.; Ko, N.; Go, Y. B.; Aratani, N.; Choi, S. B.; Choi, E.; Yazaydin, A. Ö.; Snurr, R. Q.; O'Keeffe, M.; Kim, J.; Yaghi, O. M. *Science* **2010**, *329*, 424−428.
(5) (a) O'Keeffe, M.; Peskov, M. A.; Ramsden, S. J.; Yaghi, O. M. *Acc. Chem. Res.* **2008**, *41*, 1782−1789. (b) Rajput, L.; Kim, D.; Lah, M. S. *CrystEngComm* **2013**, *15*, 259−264.
(6) Chen, B.; Eddaoudi, M.; Hyde, S. T.; O'Keeffe, M.; Yaghi, O. M. *Science* **2001**, *291*, 1021−1023.
(7) Spek, A. L. *PLATON, a multipurpose crystallographic tool*; Utrecht University Press: Utrecht, The Netherlands, 2001.
(8) (a) Ma, L.; Jin, A.; Xie, Z.; Lin, W. *Angew. Chem., Int. Ed.* **2009**, *48*, 9905−9908. (b) He, Y.-P.; Tan, Y.-X.; Zhang, J. *Inorg. Chem.* **2012**, *51*, 11232−11234.
(9) (a) Feldblyum, J. I.; Liu, M.; Gidley, D. W.; Matzger, A. J. *J. Am. Chem. Soc.* **2011**, *133*, 18257−18263. (b) Wade, C. R.; Dincă, M. *Dalton Trans.* **2012**, *41*, 7931−7938.
(10) (a) Das, S.; Kim, H.; Kim, K. *J. Am. Chem. Soc.* **2009**, *131*, 3814−3815. (b) Prasad, T. K.; Hong, D. H.; Suh, M. P. *Chem.—Eur. J.* **2010**, *16*, 14043−14050. (c) Wei, Z.; Lu, W.; Jiang, H.-L.; Zhou, H.-C. *Inorg. Chem.* **2013**, *52*, 1164−1166. (d) Wang, X.-J.; Li, P.-Z.; Liu, L.; Zhang, Q.; Borah, P.; Wong, J. D.; Chan, X. X.; Rakesh, G.; Li, Y.; Zhao, Y. *Chem. Commun.* **2012**, *48*, 10286−10288.
(11) (a) He, Y.; Krishna, R.; Chen, B. *Energy Environ. Sci.* **2012**, *5*, 9107−9120. (b) He, Y.; Zhang, Z.; Xiang, S.; Fronczek, F. R.; Krishna, R.; Chen, B. *Chem.—Eur. J.* **2012**, *18*, 613−619. (c) He, Y.; Zhang, Z.; Xiang, S.; Fronczek, F. R.; Krishna, R.; Chen, B. *Chem. Commun.* **2012**, *48*, 6493−6495. (d) He, Y.; Xiang, S.; Zhang, Z.; Xiong, S.; Fronczek, F. R.; Krishna, R.; O'Keeffee, M.; Chen, B. *Chem. Commun.* **2012**, *48*, 10856−10858. (e) Xiang, S.; Zhang, Z.; Zhao, C.-G.; Hong, K.; Zhao, X.; Ding, D.-L.; Xie, M.-H.; Wu, C.-D.; Gill, R.; Thomas, K. M.; Chen, B. *Nat. Commun.* **2012**, *2*, 204. (f) Das, M. C.; Guo, Q.; He, Y.; Kim, J.; Zhao, C.-G.; Hong, K.; Xiang, S.; Zhang, Z.; Thomas, K. M.; Krishna, R.; Chen, B. *J. Am. Chem. Soc.* **2012**, *134*, 8703−8710. (g) Zhang, Z.; Xiang, S.; Chen, B. *CrystEngComm* **2011**, *13*, 5983−5992.
(12) Bloch, E. D.; Queen, W. L.; Krishna, R.; Zadrozny, J. M.; Brown, C. M.; Long, J. R. *Science* **2012**, *335*, 1606−1610.